中国科技论文在线 http://www.paper.edu.cn

Materials Science and Engineering B98 (2003) 156–160

Raman investigation of lattice vibration modes and thermal conductivity of Nd-doped zircon-type laser crystals

Guiwu Lu [a], Chunxi Li [a,*], Wenchuan Wang [a], Zihao Wang [a], Hairui Xia [b], Peng Zhao [b]

[a] College of Chemical Engineering, Beijing University of Chemical Technology, 15 Beisanhuan-Donglu, Beijing 100029, China
[b] Department of Physics, Shandong University, Jinan 250100, China

Received 16 January 2002; received in revised form 4 December 2002; accepted 14 January 2003

Abstract

The Raman spectra of neodymium-doped yttrium orthovanadate Nd:YVO_4 (NYV) and neodymium-doped gadolinium orthovanadate Nd:$GdVO_4$ (NGV) have been measured at room temperature with different geometrical configurations. On the basis of the group theory and lattice dynamics theory, all the Raman peaks are assigned, and a correlation between the thermal conductivity and the Raman scattering strength is presented. The thermal conductivity of Nd:$GdVO_4$ and Nd:YVO_4 crystals along [1 1 0] and [1 0 1] directions are calculated and a good agreement with experimental results is obtained. The higher thermal conductivity of NGV crystal is mainly attributed to the fact that the effective radius of Gd^{3+} ion in NGV crystal is close to that of Nd^{3+} ion, which in return, enhances the crystal field strength of the laser crystal.
© 2003 Elsevier Science B.V. All rights reserved.

Keywords: Raman spectra; Laser crystal; Thermal conductivity; Space group

1. Introduction

Because of its high absorption coefficient, large emission cross-section and long fluorescence lifetime, Nd:YVO_4 (NYV) crystal has been applied in the high efficiency laser-diode pumped solid-state lasers [1]. In recent years, a new laser crystal, Nd:$GdVO_4$ (NGV), has been receiving considerable attention [2,3]. Compared with NYV, NGV crystal has almost entirely similar laser properties, but much higher absorption coefficient and larger emission cross-section [4]. Besides, most importantly, NGV crystal is characterized by its unexpectedly high thermal conductivity along [1 1 0] direction, which is comparable to that of YAG crystal [4,5].

The thermal conductivity of laser crystal is of importance from both fundamental and applied perspectives, and the dissipation of heat in high power laser devices is an important design consideration. However, despite large numbers of work, both experimental and theoretical, on optical and structural properties relatively little work has been reported on the thermal conductivity theory of laser crystal. Furthermore, it has not been understood very well why the thermal conductivity of NGV crystal is larger than that of NYV crystal. In this paper, a correlation between the thermal conductivity and the Raman scattering strength is presented according to lattice dynamics theory. The Raman spectra of neodymium-doped yttrium orthovanadate Nd:YVO_4 (NYV) and neodymium-doped gadolinium orthovanadate Nd:$GdVO_4$ (NGV) have been measured at room-temperature with different scattering configurations. On the basis of the group theory, all the Raman peaks are assigned. The thermal conductivity of Nd:$GdVO_4$ and Nd:YVO_4 crystals along [1 1 0] and [1 0 1] directions are calculated and a good agreement with experimental results is obtained.

2. Theoretical model

From lattice dynamics theory the thermal conductivity κ is given by [6]

* Corresponding author. Tel.: +86-10-6444-9190; fax: +86-10-6443-6781.
E-mail address: licx@mail.buct.edu.cn (C. Li).

0921-5107/03/$ - see front matter © 2003 Elsevier Science B.V. All rights reserved.
doi:10.1016/S0921-5107(03)00044-8

转载

中国科技论文在线 http://www.paper.edu.cn

$$\kappa = \frac{1}{3} C_v u^2 \tau, \tag{1}$$

where C_v is the lattice specific heat, u is the average velocity of sound, and τ is the phonon lifetime. Hofmeister [7] showed that optic modes could be more important to thermal conductivity κ than the acoustic modes. For molecular crystal (having s atoms in a molecule), the contribution of optic modes on the specific heat of crystal can be expressed as [8]

$$C_v = A \sum_{j=4}^{3s} x_j^2 \frac{e^{x_j}}{(e^{x_j} - 1)^2}, \tag{2}$$

where A is a constant, $x_j = h\nu_j/kT$, ν_j is the vibration frequency of normal optical mode j, h is the Plank constant and k is the Boltzman constant. At low temperature τ is relatively long and is dominated by extrinsic effects such as crystal defect and finite crystal size and $C_v \approx (T/\Theta)^3$ where Θ is the Debye temperature. As the temperature increases intrinsic temperature decided by Umklapp process become dominant, thus causing a decrease in τ. The Debye temperature of NYV crystal [9] is about 442 K. At room temperature, the dependence of τ on the concentration of doped atom is difficult to account for in detail since we are in a regime where both extrinsic and intrinsic scattering processes are important. As an approximation, we only consider the effect of extended defect on τ. The scattering of the phonons from an extended defect can be described on the basis of spherical objects scattering model, the lifetime being given by [10]

$$\tau^{-1} = \begin{cases} 4\pi^5 F^6 n u \tilde{\nu}^4 & \text{for} \quad \lambda > 2\pi F \\ \pi F^2 n u/4 & \text{for} \quad \lambda < 2\pi F \end{cases}, \tag{3}$$

where λ is wavelength of phonon, n and F are the concentration and diameter of extended defects as spherical objects. For larger extended defect in crystal, $\lambda < 2\pi F$. Thus, the dependence of κ on n can be expressed as

$$\kappa = \frac{4Au}{3nF^2\pi} \sum_{j=4}^{3s} x_j^2 \frac{e^{x_j}}{(e^{x_j} - 1)^2}. \tag{4}$$

The Raman scattering intensity (integrated intensity) of lattice mode v can be expressed as [11]

$$I(v) = K \frac{(v_0 - v)^4}{v(1 - e^{-hv/kT})}, \tag{5}$$

where K is the constant and v_0 is incident light frequency. Usually, $v/v_0 < 0.1$, we omit the items such as $(v/v_0)^2$, $(v/v_0)^3$ or higher expansion terms in Eq. (5) and obtain

$$I(x_j) = K_0 \frac{e^{x_j}(1 - 4x_j/x_0)}{x_j(e^{x_j} - 1)} \tag{6}$$

From Eqs. (4) and (6), the correlation between the thermal conductivity and Raman scattering intensity is given as follows

$$\kappa = \frac{B_0 u}{nT^2F^2} \sum_{j=4}^{3s} \frac{\tilde{\nu}_j^4}{(1 - 4\tilde{\nu}_0/\tilde{\nu}_j)^2 e^{hc\tilde{\nu}_j/kT}} I^2(\tilde{\nu}_j), \tag{7}$$

where B_0 is a constant, c is the velocity of incident light, $\tilde{\nu}_0$ is the wavenumber of incident laser ν_0, and $\tilde{\nu}_j$ is the wavenumber of lattice vibration mode ν_j.

3. Crystal preparation and analysis of normal modes

The single crystals of NYV and NGV, obtained from State Key Lab of Crystal Materials of Shandong University, were cut carefully along a-, b-, and c-axes with a precision of 1′, then were optically polished, with the size of about $9 \times 9 \times 12$ mm^3 and $8 \times 8 \times 10$ mm^3, respectively. Raman spectra were measured on a SPEX-1403 Raman spectrometer, using a 300-mW argon ion laser at 514.5 nm with a power density of 1.8 W cm^{-2} at the sample. Raman spectra were collected three times with a resolution of 0.15 cm^{-1} and a precision of 1 cm^{-1} in the frequency range from 50 to 1000 cm^{-1}.

Uniaxial crystals NYV and NGV crystallized with a zircon-type structure in the tetragonal system, conforming to the space group $I4_1/amd$ at room-temperature. As the unit cell contains two VO_4^{3-} anions and two Y^{3+} (or Gd^{3+} or Nd^{3+}) cations, the factor group analysis shows that there are in total 36 normal modes classified as follows [12]:

$$\Gamma = 2A_{1g} + 1A_{1u} + 1A_{2g} + 4A_{2u} + 4B_{1g} + 1B_{1u} + 1B_{2g} + 2B_{2u} + 5E_g + 5E_u.$$

The classification into acoustic, optical translational, optical rotatory and internal modes is summarized in Table 1. According to Table 1, the Raman- and Infrared active optic phonon modes are obtained as follows:

Table 1
Classification of the modes in zircon crystal

D_{4h}	N	T_A	T	R	I	Raman-active	IR-active
A_{1g}	2	0	0	0	2	$\alpha_{xx}+\alpha_{yy}$, α_{zz}	
A_{2g}	1	0	0	1	0		
B_{1g}	4	0	2	0	2	$\alpha_{xx}-\alpha_{yy}$	
B_{2g}	1	0	0	0	1	α_{xy}	
E_g	5	0	2	1	2	α_{xz}, α_{yz}	
A_{1u}	1	0	0	0	1		
A_{2u}	4	1	1	0	2		e_z
B_{1u}	1	0	0	1	0		
B_{2u}	2	0	0	0	2		
E_u	5	1	1	1	2		e_x, e_y

N, T_A, T, R, and I are number of total, acoustic, translational, librational and internal modes, respectively.

中国科技论文在线 http://www.paper.edu.cn

$$\Gamma_{Vib} = 2A_{1g}(R) + 4B_{1g}(R) + 1B_{2g}(R) + 5E_g(R) + 3A_{2u}(IR) + 4E_u(IR). \quad (8)$$

It is clear that theoretically observable Raman peaks and infrared reflection bands are not more than 17 and 11 in number, respectively. The Raman scattering tensors are [13]

$$A_{1g} = \begin{bmatrix} a & 0 & 0 \\ 0 & a & 0 \\ 0 & 0 & b \end{bmatrix}, B_{1g} = \begin{bmatrix} c & 0 & 0 \\ 0 & -c & 0 \\ 0 & 0 & 0 \end{bmatrix}, B_{2g} = \begin{bmatrix} 0 & d & 0 \\ d & 0 & 0 \\ 0 & 0 & 0 \end{bmatrix},$$

and

$$E_g = \begin{bmatrix} 0 & 0 & e \\ 0 & 0 & 0 \\ e & 0 & 0 \end{bmatrix} + \begin{bmatrix} 0 & 0 & 0 \\ 0 & 0 & e \\ 0 & e & 0 \end{bmatrix}.$$

Because of equivalence of the axes X and Y for the measurement of Raman spectra of the non-polar modes of uniaxial crystals with the point group 4/mmm, the interesting geometrical configurations are X(ZZ)Y, X(YY)Z, X(YX)Y and Z(YZ)X, corresponding to the symmetry species A_{1g}, $(A_{1g}+B_{1g})$, B_{2g}, and E_g, respectively.

4. Experimental results and discussion

Non-polar lattice vibration modes, belonging to the symmetry species A_{1g}, were observed in NYV and NGV crystal at room-temperature with X(ZZ)Y scattering geometry, and the spectra in a frequency range from 50 to 1000 cm^{-1} are shown in Fig. 1. For NYV crystal, two Raman-active optical phonon modes at 380 cm^{-1} (v_2) and 895 cm^{-1} (v_1) were recorded. Compared with Raman spectra [14] of the aqueous solution of VO_4^{3-} ion, the v_1 and v_2 can be assigned as a V–O stretching vibration mode and an in-plane O–V–O bending vibration mode, respectively. For NGV crystal, two Raman-active optical phonon modes at 380 (v_2) and 887 cm^{-1} (v_1) were recorded in Fig. 1(b).

Fig. 2 shows Raman spectra of NYV and NGV crystals for the X(YY)Z scattering configuration, which corresponds to the symmetry species $(A_{1g}+B_{1g})$. Compared scattering lines of X(YY)Z with that of X(ZZ)Y, the B_{1g} symmetry species Raman lines recorded for NYV crystal are 161, 263, 492, and 821 cm^{-1}; for NGV crystal are 156, 246, 263, 484, and 813 cm^{-1}.

In Fig. 3, we assign the band at 264 cm^{-1} as B_{2g} mode for NYV and NGV crystals. The spectra bands of 824 cm^{-1} (for NYV) and 814 cm^{-1} (for NGV) are spillover resulting from slight misalignment of the crystals or scattering from crystal defects. Fig. 4 shows Raman spectra of NYV and NGV crystals corresponding to E_g species modes. For NYV crystal, five Raman-active modes were already recorded as 166, 262, 494, 819 and 922 cm^{-1}; for NGV crystal, they are 156, 246, 485, 811 and 913 cm^{-1}.

In the NYV and NGV crystal, the 4b site is four coordinated. In a crystallographic cell there are four V–O tetrahedral configurations, each having four oxygen-ion neighbors at the V–O distance of 0.1706 nm. The 4a site is four coordinated and in a crystallographic cell there are four YO_8 (or GdO_8 or NdO_8) dodecahedral

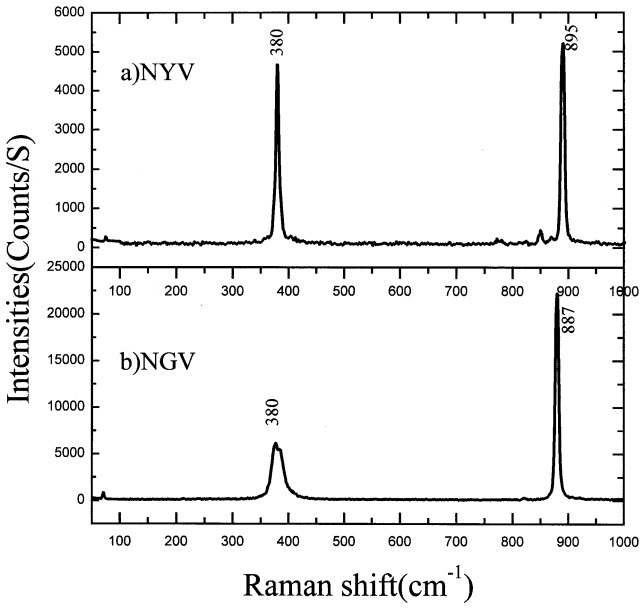


Fig. 1. Raman spectra of NYV and NGV at room temperature for the symmetry species A_{1g} with the scattering configurations X(ZZ)Y.

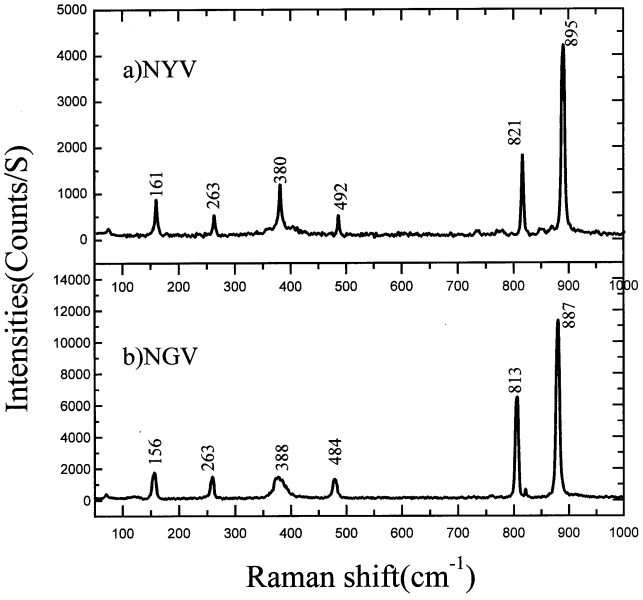


Fig. 2. Raman spectra of NYV and NGV at room temperature for the symmetry species $(A_{1g}+B_{1g})$ with the scattering configurations X(YY)Z.

中国科技论文在线 http://www.paper.edu.cn

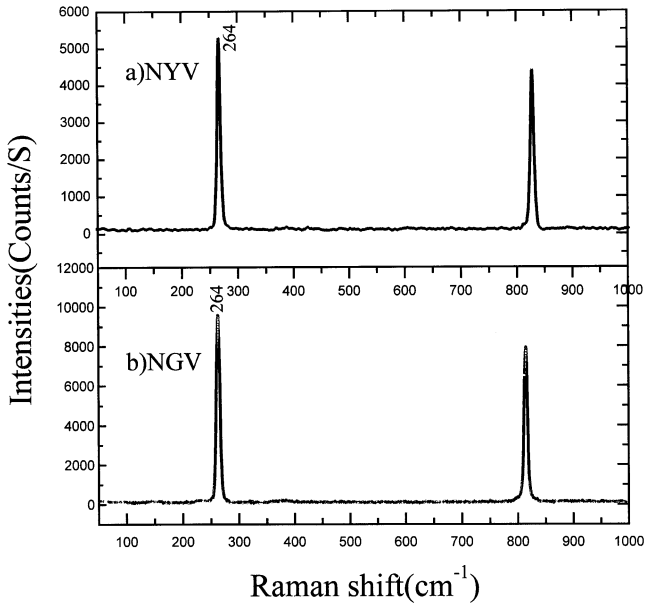


Fig. 3. Raman spectra of NYV and NGV at room temperature for the symmetry species B_{2g} with the scattering configurations X(YX)Y.

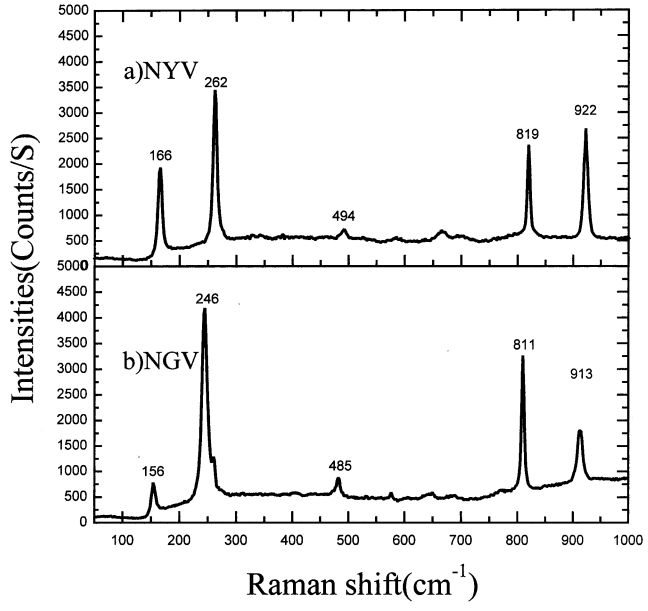


Fig. 4. Raman spectra of NYV and NGV at room temperature for the symmetry species E_g with the scattering configurations Z(YZ)X.

configurations, each having four nearest oxygen-ion neighbors and four next-nearest oxygen-ion neighbors. In general, the difference of ion radius between doped-ion and host-ion may cause deformation or distortion of molecule cluster in crystal, which in return, changes the crystal field and the Raman scattering intensity. Keeping in mind that the effective radius of Gd^{3+} ion is 0.111 nm that is close to that of Nd^{3+} ion (0.115 nm), but the effective radius of Y^{3+} ion (0.106 nm) is much smaller than that of Nd^{3+} ion. Therefore, the crystal field strength in NGV is larger than that in NYV crystal, and this may be the reason that Raman-active mode strength recorded for Nd:$GdVO_4$ is stronger than that for Nd:YVO_4 crystal (Figs. 1, 2 and 4).

All the Raman peaks observed in our experiment are assigned in Table 2, while the variety of Raman scattering intensity and the red-shift of wavenumber are also compared. It is easy to see that the red-shift of stretching modes of GdO_8 and VO_4 clusters is more significant than that of bending modes (Table 2). The fact that the mass of Gd atom is larger almost two times than that of Y atom, can explain red-shift of Raman lines in NGV crystal. From Table 2, we can find that the scattering intensities of Raman-active modes in NGV crystal are related to the scattering geometry projects. For example, the scattering intensity of 880 cm^{-1} mode of NGV crystal is about 22 000 Counts s^{-1} for X(ZZ)Y project; however, it decreases to about 12 000 Counts s^{-1} for X(YY)Z project. These results indicate that the anisotropy of GdO_8 and VO_4 clusters in NGV crystal is enhanced, thus the thermal conductivity has an obvious change along different directions.

The thermal conductivity ratio of $\kappa_{NGV}/\kappa_{NYV}$ is calculated using Eq. (7) and the calculated results are listed in Table 3. For X(ZZ)Y and X(YX)Y scattering projects, the phonon propagates along [1 1 0] direction, thus the $\kappa_{NGV}/\kappa_{NYV}$ along [1 1 0] direction is calculated to be 1.935 and 2.025, respectively. For X(YY)Z and Z(YZ)X scattering projects, the $\kappa_{NGV}/\kappa_{NYV}$ along [1 0 1] direction is calculated to be 1.225 and 1.143, respectively. The calculated results agree well with experiment results [4,15].

In this paper, we only consider the effect of extended defect on the phonon lifetime τ. In fact, IR reflectance and Raman spectra implicitly contain information on the lifetimes of the vibration modes (i.e. $\tau = 1/2\pi$FWFM, where FWFM is the full width of the peak at half maximum), if phonon–phonon interactions are accounted for [16,17]. Recently, Hofmeister [18] has successfully calculated thermal conductivity of spinels and olivines using Raman spectra method. Her model can be extended directly into zircon-type laser crystals. This work is carrying out in our laboratory and the results will be reported in future paper.

5. Conclusion

We have measured the Raman spectra of Nd:YVO_4 and Nd:$GdVO_4$ crystals at room-temperature, and assigned all the Raman peaks using space group theory and lattice dynamics theory. The broadening and splitting of Raman lines are related to the crystal field strength in NGV crystal, which is much stronger than that in NYV crystal. For the optical lattice vibration modes, a correlation between the thermal conductivity

中国科技论文在线 http://www.paper.edu.cn

Table 2
The assignment of the normal vibration modes of NYV and NGV crystals

Raman shift (cm^{-1})		I_{NGV}/I_{NYV}	Red-shift	Symmetry	Approximately
NYV	NGV		$(\tilde{v}_{NYV}-\tilde{v}_{NGV})$	species	description
161	156	0.225	5	B_{1g}	O–Gd(Y)–O bend
166	156	0.312	10	E_g	$Gd(Y)O_8$ bend
262	246	0.741	16	E_g	$Gd(Y)O_8$ stretch
263	263	0.832	17	B_{1g}	$Gd(Y)O_8$ stretch
264	264	1.22	0	B_{2g}	NdO_8 stretch
380	380	1.33	0	A_{1g}	v_2, O–V–O bend
492	484	1.33	6	B_{1g}	
494	485			E_g	
819	811	0.832	8	E_g	VO_4 symmetry stretch
821	813	1.45	8	B_{1g}	VO_4 symmetry stretch
824	814	0.854	10		spillover
895	887	1.31	8	A_{1g}	v_1, VO_4 asymmetry stretch
922	913	1.12	9	E_g	v_1, VO_4 asymmetry stretch

Rotatory and internal modes.

Table 3
The calculated thermal conductivity ratio ($\kappa_{NGV}/\kappa_{NYV}$)

Phonon propagation direction		[1 1 0]		[1 0 1]	
Scattering projects		X(ZZ)Y	X(YX)Y	X(YY)Z	Z(YZ)X
$\kappa_{NGV}/\kappa_{NYV}$	Calculation	1.935	2.025	1.225	1.143
	Experiment [15]	1.9 ± 0.2		1.1 ± 0.1	

and the Raman scattering strength is presented, and the thermal conductivity ratio of Nd:$GdVO_4$ and Nd:YVO_4 crystals along [1 1 0] and [1 0 1] directions are calculated respectively for the first time. The higher thermal conductivity of NGV crystal is mainly attributed to the increase of atom mass and radius compared with NYV crystal, which in return, changes anisotropy of molecular clusters and the crystal field strength in laser crystal. In the future study, we consider that choosing Gd-like ion (with large effective radius and heavy atom mass) as host ion may obtain inspiring discovery.

Acknowledgements

This work is supported by Natural Science Foundation of China (No. 20076001 and No. 20236010).

References

[1] T. Jensen, V.G. Ostroumov, J.P. Meyn, G. Huber, A.I. Zagumennyi, I.A. Shcherbakov, Appl. Phys. B 58 (1994) 373.
[2] K. Shimamura, S. Uda, V.V. Kochurikhin, T. Taniuchi, T. Fukuda, Jpn J. Appl. Phys. 35 (1996) 1832.
[3] H.J. Zhang, X.L. Meng, L. Zhu, H.Z. Zhang, P. Wang, J. Dawes, C.Q. Wang, Y.T. Chow, Cryst. Res. Technol. 33 (1998) 801.
[4] P.A. Studenikin, A.J. Zagumennyi, Y.D. Zavartsev, P.A. Popov, I.A. Shcherbakov, Quantum Electron 25 (1995) 1162.
[5] D.Y. Shen, H.R. Yand, J.G. Liu, S.C. Tam, Y.L. Lam, W.J. Xie, J.H. Gu, K. Ueda, Appl. Phys. B 72 (2001) 263.
[6] D.I. Florescu, V.M. Asnin, Fred H. Pollak, R.J. Molnar, C.E.C. Wood, J. Appl. Phys. 88 (2000) 3295.
[7] A.M. Hofmeister, Science 283 (1999) 1699.
[8] R. Fowler, E.A. Guggenheim, Stat. Thermodynamics (1952) 151.
[9] R.J. Wang, F.Y. Li, X. Wu, H.G. Yang, Chinese J. Laser 27 (2000) 449.
[10] J.E. Graebner, M.E. Reiss, L. Seibles, T.M. Hartnett, R.P. Miller, C.J. Robinson, Phys. Rev. B 50 (1994) 3702.
[11] K. Nakamoto, Infrared and Raman Spectra of Inorganic and Coordination Compounds, third ed., Wiley, 1978, p. 83.
[12] P. Dawson, M.M. Hargreave, G.R. Wilkinson, J. Phys. C: Solid State Phys. 4 (1971) 240.
[13] R. Loudon, Adv. Phys. 13 (1964) 423.
[14] N. Weinstock, H. Schulze, A. Muller, J. Chem. Phys. 59 (1973) 5063.
[15] S. Tian, The Handbook of Functional Material and Application, Mechanics Industry Publishing Company, Beijing, 1996, p. 587.
[16] L.J. Tassie, The Physics of Elementary Particles, Longman, London, 1973, p. 217.
[17] A.M. Hofmeister, H.K. Mao, Am. Mineralogist 86 (2001) 622.
[18] A.M. Hofmeister, Am. Mineralogist 86 (2001) 1188.